3rd China-Japan Joint Workshop on Positron Science (JWPS2017)
JJAP Conf. Proc. **7**, 011004 (2018) https://doi.org/10.7567/JJAPCP.7.011004

Coupled Channel Study of Antihydrogen-hydrogen Molecular Resonance State

Takuma Yamashita and Yasushi Kino

Department of Chemistry, Tohoku University, Sendai 980-8578, Japan

E-mail: t.ymst@dc.tohoku.ac.jp

(Received March 31, 2018)

We report a theoretical study of antihydrogen-hydrogen molecular resonance states consisting of a positron, an antiproton, an electron and a proton. The four particles strongly correlate and show different character from the hydrogen molecule. Because of the non-separability of the positron and electron motions from the antiproton and proton motions, the adiabatic approximation breaks down at the short antiproton-proton distance. Based on a non-adiabatic method, we directly solve the four-body problem and obtain the resonance energies and widths. In order to examine the roles of positron-antiproton and electron-proton correlations as well as positron-electron and antiproton-proton correlations, we introduce two different types of coordinate systems. One is suited for describing an antihydrogen-hydrogen configuration, and the other is a positronium-protonium configuration. The antihydrogen-hydrogen configuration contributes to the existence of the molecular resonance states, and the positronium-protonium configuration makes the resonance states unstable. Mixing of the two configurations results in an antihydrogen-hydrogen molecular resonance state, and the resonance state has an energy of −0.077 9(3) a.u. from the antihydrogen-hydrogen dissociation threshold with its lifetime 16 (2) fs.

1. Introduction

Formation of a compound of matter and antimatter has been a subject of interest in nuclear physics, atomic physics, quantum chemistry and material sciences [1–4] because the annihilation of antiparticles gives microscopic information about the momentum and position of the counter particles. In order to carry out precise tests for symmetry between antimatter and matter, cutting-edge technologies such as ultra-high vacuum, high radiation-resistant detectors, precise control of electromagnetic fields and so on are necessary. Confined antiparticles in ultra-high vacuum may cause unfavorable reactions with electrons or nuclei of atoms in impurity gas, and emits signals that can be detected outside with high-efficiency. In other words, antimatter experiments can be a strict test of these technologies. Moreover, theoretical studies play an important role in interpreting such experiments.

Since annihilation cross sections are much smaller than the size of the H atom, annihilation effects are less dominant than atomic collision process. A complex of antimatter and matter would show exotic structures and characteristics under the balance of opposite sign of Coulombic force.

A positronic atom, a bound state of a positron and a neutral atom, is a simple compound of an antimatter particle and matter atom. It has been pointed out that the positron cannot form a bound state with a neutral hydrogen atom and helium atom; therefore, the simplest positronic atom is a positronic lithium atom (e^+Li) whose electronically stable bound state was theoretically proved by a precise calculation in 1997 [5, 6]. Theoretical investigations performed since then have revealed that positronium (Ps, a bound state of e^+ and e^-) formation by configuration rearrangement can contribute to the binding mechanism of the positronic atoms [7–11]. A host atom like lithium, whose ionization energy is smaller than the binding energy of positronium, can capture the Ps by the electric field of the residual ion. On the other hand, if the ionization energy of the host atom is larger than the binding

energy of Ps, the formation of Ps is less dominant, but can indirectly contribute to the binding energy.

The second step to explore matter-antimatter compounds will be represented by a system involving two antiparticles. Recently by using an intense positron beam, Ps_2 consisting of two positrons and two electrons was observed in an experiment [12]. Another two-antiparticle system is the antihydrogen atom ($\overline{H}$) which is made of an antiproton and a positron. Experimental techniques to confine and control cold antihydrogen atoms have become more sophisticated recently [13–16], and precise spectroscopy [17–19] is making remarkable progress. Free-fall experiments [20, 21] are also upcoming.

The minimum matter-antimatter compound consists of $\overline{H}$ and H. The compound is expected to have molecular states below the dissociation threshold of $\overline{H}$ (1s) + H (1s) similar to H_2 and PsH molecules [22–27] because of an attractive interaction between the $\overline{H}$ and H. In the molecular states, however, a protonium (Pn, a bound state of $\overline{p}$ and p) and a positronium can be formed by a configuration rearrangement reaction. The size of the Pn (1s) state is about 900 times smaller than that of H (1s) and the dipole moment of the Pn (1s) is too small to form a bound state with Ps (1s). Thus, the molecular states are not true bound states like PsH and H_2 but resonance states. In the present paper, we call the resonance states located below $\overline{H}$ (1s) + H (1s) molecular resonance states $\overline{H}H$ in analogy with H_2.

$\overline{H}H$ dissociates into fragments by the configuration rearrangement reaction,

$$\overline{H}H \rightarrow Ps + Pn. \tag{1}$$

$\overline{H}H$ has been investigated by theoretical calculations based on the adiabatic (Born-Oppenheimer) framework [28] where the motions of the electrons and positrons (light particles) are calculated separately from those of the nuclei (heavy particles). However, the attractive interaction between the antiproton and proton accelerates the speed of the nuclei up to that of the positron and electron and the adiabatic framework breaks down at short inter-nuclear distance. Recently, resonance energies and widths below the dissociation threshold of $\overline{H}$ (1s) + H (1s) were calculated [29] with a non-adiabatic calculation, the Gaussian expansion method (GEM) [30]. The reported resonance energies are somewhat close to the adiabatic energy levels. An investigation on weights of the wavefunction by Stegeby and Piszczatowski [29] suggests an intriguing aspect on the mechanism and structure of the resonance states and admits further studies. In the present paper, we investigate the role of the inter-particle correlations, 'positron-antiproton and electron-proton' and 'positron-electron and antiproton-proton' correlations, in the $\overline{H}H$ resonance states by analyzing the energy levels by a coupled channel study [27, 31, 32] using GEM. We use simple coupled-channel trial wavefunctions due to the limit of computation cost, and calculate resonances by a complex scaling method [33].

Atomic units (a.u.; $m_e = \hbar = e = 1$) are used throughout this paper, except where mentioned otherwise.

2. Theory

The total Hamiltonian for $\overline{H}H$ is written as

$$H = \hat{K}_{\overline{p}} + \hat{K}_p + \hat{K}_{e^+} + \hat{K}_{e^-} - \hat{K}_{CM} - \frac{1}{r_{\overline{p}e^+}} - \frac{1}{r_{pe^-}} - \frac{1}{r_{e^+e^-}} - \frac{1}{r_{\overline{p}p}} + \frac{1}{r_{\overline{p}e^-}} + \frac{1}{r_{pe^+}}, \tag{2}$$

where $\hat{K}_x$ (x = {$\overline{p}$, p, e^+, e^-}) is a kinetic energy operator associated with position vector of particle x, $\hat{K}_{CM}$ is the kinetic energy operator for the center of mass of the system and r_{xy} is inter-particle distance between x and y. The Schrödinger equation is given by

$$H\Psi_{J\upsilon} = E_{J\upsilon}\Psi_{J\upsilon}, \tag{3}$$

where $E_{J\upsilon}$ is the eigenenergy of the υ-th eigenstate with total angular momentum J. Since we focus on the S-wave resonance states, we set $J = 0$. We hereafter omit J and υ for simplicity. In the GEM,

the totalwavefunction Ψ is described as a summation of channel wave functions ψ_c. In the present paper, we introduce two different Jacobian coordinate systems $c = 1, 2$ shown in Fig. 1. The first channel $c = 1$ is suitable to describe the $\overline{\mathrm{H}}$ + H configuration and the second one $c = 2$ is suitable to describe an alternative configuration, Pn + Ps. The channel wavefunction ψ_c is expanded in terms of Gaussian functions. The explicit forms for $\psi_{c=1}$ and $\psi_{c=2}$ are respectively given as

$$\psi_{c=1}(r_1, r_2, r_3) = \sum_{n_{c,1}=1}^{N_{c,1}} \sum_{n_{c,2}=1}^{N_{c,2}} \sum_{n_{c,3}=1}^{N_{c,3}} A_{n_{c,1},n_{c,2},n_{c,3}} \exp\left(-\frac{r_1^2}{\alpha_{c,n_{c,1}}^2} - \frac{r_2^2}{\beta_{c,n_{c,2}}^2} - \frac{r_3^2}{\gamma_{c,n_{c,3}}^2}\right) \cos\left(\zeta \frac{r_3^2}{\gamma_{c,n_{c,1}}^2}\right) + \sum_{n_{c,1}=1}^{N_{c,1}} \sum_{n_{c,2}=1}^{N_{c,2}} \sum_{n_{c,3}=1}^{N_{c,3}} B_{n_{c,1},n_{c,2},n_{c,3}} \exp\left(-\frac{r_1^2}{\alpha_{c,n_{c,1}}^2} - \frac{r_2^2}{\beta_{c,n_{c,2}}^2} - \frac{r_3^2}{\gamma_{c,n_{c,3}}^2}\right) \sin\left(\zeta \frac{r_3^2}{\gamma_{c,n_{c,1}}^2}\right), \quad (4)$$

and

$$\psi_{c=2}(R_1, R_2, R_3) = \sum_{n_{c,1}=1}^{N_{c,1}} \sum_{n_{c,2}=1}^{N_{c,2}} \sum_{n_{c,3}=1}^{N_{c,3}} A_{n_{c,1},n_{c,2},n_{c,3}} \exp\left(-\frac{R_1^2}{\alpha_{c,n_{c,1}}^2} - \frac{R_2^2}{\beta_{c,n_{c,2}}^2} - \frac{R_3^2}{\gamma_{c,n_{c,3}}^2}\right) \cos\left(\zeta \frac{R_1^2}{\alpha_{c,n_{c,1}}^2}\right) + \sum_{n_{c,1}=1}^{N_{c,1}} \sum_{n_{c,2}=1}^{N_{c,2}} \sum_{n_{c,3}=1}^{N_{c,3}} B_{n_{c,1},n_{c,2},n_{c,3}} \exp\left(-\frac{R_1^2}{\alpha_{c,n_{c,1}}^2} - \frac{R_2^2}{\beta_{c,n_{c,2}}^2} - \frac{R_3^2}{\gamma_{c,n_{c,3}}^2}\right) \sin\left(\zeta \frac{R_1^2}{\alpha_{c,n_{c,1}}^2}\right). \quad (5)$$

The linear parameters $A_{n_{c,1},n_{c,2},n_{c,3}}$ and $B_{n_{c,1},n_{c,2},n_{c,3}}$ are determined by the variational principle for eigenenergies. The non-linear parameters $\alpha_{c,n_{c,1}}$, $\beta_{c,n_{c,2}}$ and $\gamma_{c,n_{c,3}}$ are given according to the geometrical progression to describe both short-range correlation and long-range tail behavior. In order to avoid numerical error caused by non-orthogonality of Gaussian functions, we here introduce Gaussian functions multiplied by cosine and sine functions. In the present case, we optimize the parameter to be $\zeta = 1.5$.

The total wavefunction is written in the form of a coupled channel wavefunction,

$$\Psi = \psi_{c=1}(r_1, r_2, r_3) + \psi_{c=2}(R_1, R_2, R_3). \quad (6)$$

The mixing of the two functions $\psi_{c=1}(r_1, r_2, r_3)$ and $\psi_{c=2}(R_1, R_2, R_3)$ can facilitate inter-particle correlations in the molecular resonance states $\overline{\mathrm{H}}\mathrm{H}$. Near the $\overline{\mathrm{H}}$ (1s) + H (1s) dissociation threshold

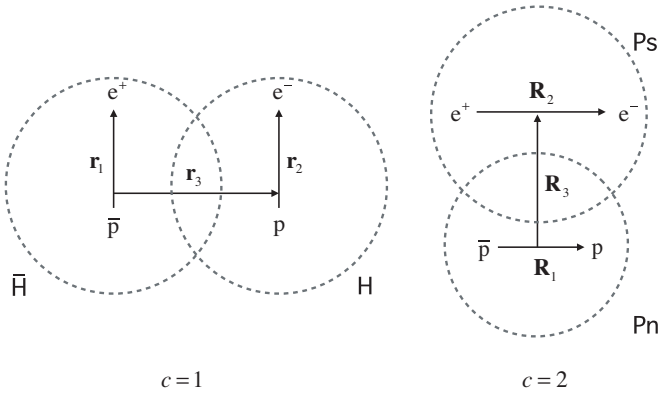

Fig. 1 Two types of Jacobian coordinate systems for $\overline{\mathrm{H}}\mathrm{H}$. Circles demonstrate schematic views of $\overline{\mathrm{H}}$, H, Ps and Pn. The size of the circle of Pn illustrates a situation that Pn (25s) state has ∼ 1 a.u. for the expectation value of diameter which is smaller than that of $\overline{\mathrm{H}}$ (1s), H (1s), Ps (1s).

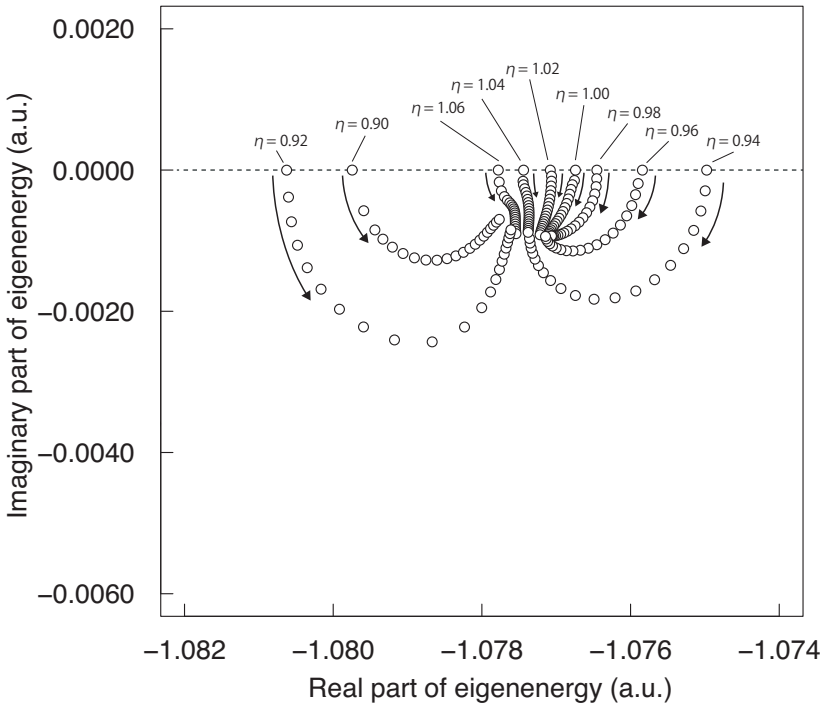

Fig. 2 Complex scaling trajectories as a function of θ ($\Delta\theta = 0.005$) using η parameter. The corresponding η parameter is noted by an eigenvalue calculated with $\theta = 0$. θ increases in the direction of the arrows. From the stationary point of the trajectories, the resonance state is found at $E_r = -1.077\,4\,(3)$ and $\Gamma = 0.001\,6\,(3)$.

($E_{th} = -0.999\,456$), rearrangement dissociation thresholds to Ps ($n = 2$) + Pn ($n = 22$) ($E_{th} = -1.010\,926$) and Ps ($n = 1$) + Pn ($n = 25$) ($E_{th} = -0.984\,461$), are located. Therefore, the channel function $\psi_{c=2}(R_1, R_2, R_3)$ is required to reproduce excited states of the Pn ($n < 30$). Numbers of Gaussian range parameters for r_3 and R_1 appeared in Eqs. (4) and (5) is set to be more than 120 to reproduce many nodes in the wavefunctions of the excited states.

Resonance energies and widths are determined by a complex scaling method [33]. A complex dilation operator is defined as

$$U(\eta, \theta) f(\mathbf{r}) = \eta^{\frac{3}{2}} e^{\frac{3}{2} i\theta} f(\eta e^{i\theta} \mathbf{r}), \tag{7}$$

where $f(\mathbf{r})$ is an arbitrary function of a position vector $\mathbf{r}$, and η and θ are positive real numbers for complex scaling. A complex scaled Schrödinger equation is given as

$$U(\eta, \theta) H U(\eta, \theta)^{-1} \Psi(\eta, \theta) = E(\eta, \theta) \Psi(\eta, \theta), \tag{8}$$

where $E(\eta, \theta)$ is a complex eigenenergy and $\Psi(\eta, \theta) = U(\eta, \theta)\Psi$ is a complex-scaled total wavefunction. After the complex scaling, eigenenergies for the bound states do not change, but those for continuum states rotate θ on the dissociation threshold point in the complex energy plane. For the resonance states which have natures of both bound and scattering states, eigenenergies firstly rotate and then reach a stationary point. The resonance energy E_r and width Γ are determined as $E(\eta, \theta') = E_r - i\Gamma/2$ when

$$\left. \frac{\partial E(\eta, \theta)}{\partial \theta} \right|_{\theta = \theta'} \approx 0 \tag{9}$$

is satisfied.

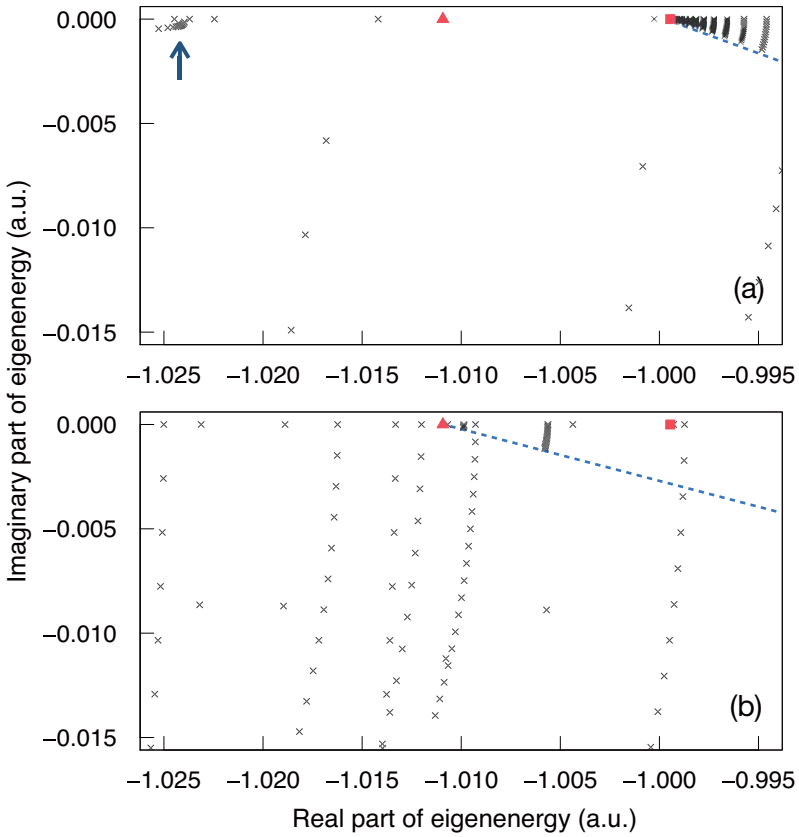

Fig. 3 Complex scaling trajectories as a function of θ ($\Delta\theta = 0.01$) with (a) $\Psi^{(c=1)}$ and (b) $\Psi^{(c=2)}$ using $\eta = 1$. The closed red box is the dissociation threshold of $\overline{\mathrm{H}}$ (1s) + H (1s), the closed red upper triangle is the dissociation threshold of Ps ($n = 2$) + Pn ($n = 22$). The dashed lines rotated on each dissociation threshold by -2θ show θ-rotated continuum states associated with the dissociation threshold. An arrow denotes the stationary point for the change in θ.

3. Results and discussion

We obtain a resonance state below the $\overline{\mathrm{H}}$ (1s) + H (1s) dissociation threshold; the threshold energy is $E_{\mathrm{th}} = -0.999\,456$. The complex scaling trajectories are shown in Fig. 2. Nine trajectories reach stationary points which satisfy Eq. (9), and the resonance energy and width are determined at the point ($E_{\mathrm{r}} = -1.077\,4\,(3)$ and $\Gamma = 0.001\,6\,(3)$). The η parameters are chosen to make the trajectories reach the stationary point from different directions. The discrepancy in the stationary points gives the error of the resonance energy and width shown in parentheses. The interval of the θ parameter, $\Delta\theta$, is chosen to make intervals of enigenenergies much smaller than the desired precision near the stationary point. The resonance energy $E_{\mathrm{r}} = -1.077\,4\,(3)$ is close to the 24th vibrational state in the adiabatic framework [28], whose energy is $E_{\mathrm{BO}} = -1.091$. Although the adiabatic framework cannot calculate the width because it cannot include the positron and electron in the continuum state, the non-adiabatically calculated width gives a lifetime of this resonance state, $\tau = 1/\Gamma = 16\,(2)$ fs.

For the analysis of $\overline{\mathrm{H}}\mathrm{H}$, we investigate the complex scaling trajectories by examining the contribution of each of the channel wavefunctions. First, we use the following trial wavefunction

$$\Psi^{(c=1)} = \psi_{c=1}\,(r_1,\, r_2,\, r_3). \tag{10}$$

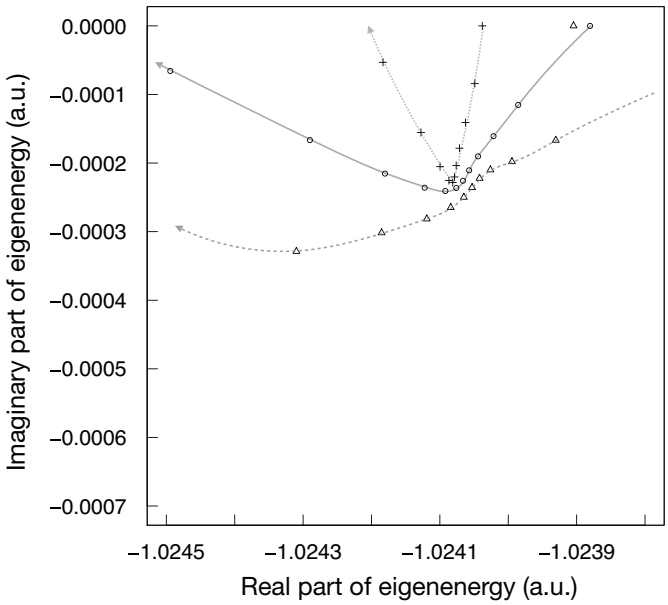

Fig. 4 Complex scaling trajectories as a function of θ ($\Delta\theta = 0.02$) with $\Psi^{(c=1)}$ using $\eta = 1$. The circle symbol with solid line, triangle symbol with dashed line and cross symbol with dotted line are the series with $\eta = 1.00$, 1.02 and 1.04, respectively.

Complex scaling trajectories near the dissociation threshold $\overline{\mathrm{H}}$ (1s) + H (1s) calculated by $\Psi^{(c=1)}$ with $\eta = 1$ is shown with a step $\Delta\theta = 0.01$ in Fig. 3 (a). The wave function given in Eqs. (4) and (5) vanish in the asymptotic region where $r \to \infty$, the continuum eigenenergy distribution for scattering states becomes a discretized distribution consisting of so-called continuum-discretized states. Since resonance states are embedded in the scattering states (continuum states), we need to distinguish the resonance states from the discretized states. Above the dissociation threshold (red square in Fig. 3 (a)), the complex scaling trajectories which rotate on the dissociation threshold with the angle of θ indicate the continuum-discretized states. We can see a stationary point for the change in θ at $-1.024\,2\,(2) - 0.000\,20\,(5)i$. Other series of the states are also discretized-continuum states associated with lower dissociation threshold. A close-up view of the complex scaling trajectories near the stationary point at $-1.024\,2\,(2) - 0.000\,20\,(5)i$ is shown in Fig. 4. The resonance widths calculated with $\Psi^{(c=1)}$ are always smaller than those with $\Psi = \psi_{c=1} + \psi_{c=2}$ because $\psi_{c=2}$ describes the dissociation states, Ps (1s) + Pn (ns), where n is a principal quantum number.

In order to examine the role of the Ps + Pn configuration for the formation of molecular resonance states, we calculate the complex eigenenergies using the second trial wavefunction defined by the $c = 2$ coordinate system

$$\Psi^{(c=2)} = \psi_{c=2}\,(R_1,\, R_2,\, R_3). \tag{11}$$

The calculated complex eigenenergies are shown in Fig. 3 (b). We can see that the continuum-discretized states rotate -2θ on the Ps ($n = 2$) + Pn ($n = 22$) dissociation threshold (red triangle symbol). In contrast to the calculation with $\Psi^{(c=1)}$, no stationary point is found in the energy region between -1.025 a.u. and -0.995 a.u.; namely, all states shown in Fig. 3 (b) are in the continuum. This could be because the spherical but highly excited Pn states whose size is ~ 1 a.u. described in $\Psi^{(c=2)}$ cause only a weak attractive interaction between the Ps and Pn.

Finally, we comment on the channel functions $\Psi^{(c=1)}$ and $\Psi^{(c=2)}$ in the hydrogen molecule. In the hydrogen molecule, $\Psi^{(c=1)}$ would play a similar role as in $\overline{\mathrm{H}}\mathrm{H}$ while there is no explicit channel de-

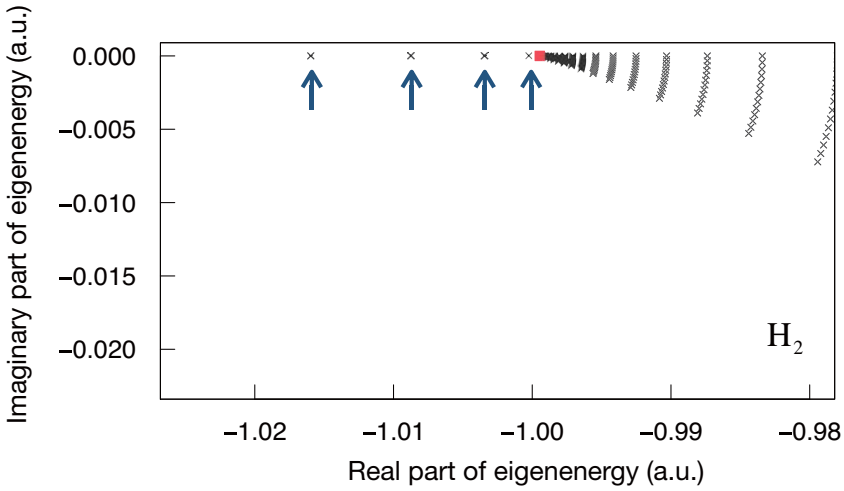

Fig. 5 Complex scaling trajectories as a function of θ ($\Delta\theta = 0.01$) for H_2 molecule with $\Psi^{(c=1)}$ using $\eta = 1$. The closed red box is the dissociation threshold of H (1s) + H (1s), arrows denote stationary points for the change in θ.

scribed by $\Psi^{(c=2)}$. When we adopt the same trial function $\Psi^{(c=1)}$ to the calculation of the H_2 molecule by replacing the particles $\{\overline{p}, e^+\}$ by $\{p, e^-\}$, the complex scaling trajectories show a different spectrum from $\overline{H}H$ as shown in Fig. 5. Here we treat the four constituent particles to be non-identical for the comparison with $\overline{H}H$. Namely, in the present calculation, we distinguish the two protons and electrons, respectively. Since the eigenstates of H_2 located below the H (1s) + H (1s) dissociation threshold are true bound states, the complex eigenenergies stay at the points on the real axis with increasing θ and η. We can find several stationary points accumulating to the dissociation threshold on the real axis and the rotation spectra of the continuum-discretized states of H (1s) + H (1s) above the dissociation threshold. This accumulating spectrum is convincing because the major interaction between the two hydrogen atoms are characterized by a long range attractive potential. The interval of the stationary points of H_2 is much smaller than that of $\overline{H}H$ though the Van der Waals interaction between $\overline{H}$ and H is the same as that between H and H. This suggests that the attractive interaction between the two atoms have a shorter range in $\overline{H}H$ than in H_2. This suggestion is consistent with the result that the adiabatic potential of H_2 [34] is deeper than that of $\overline{H}H$ [35] outside 1.5 a.u.

4. Conclusion

We report a coupled channel study of molecular resonance states of $\overline{H}H$ below the $\overline{H}$ (1s) + H (1s) dissociation threshold based on a non-adiabatic treatment. A complex scaling method is adopted to calculate the resonance states. A coupled channel wavefunction that includes two possible configurations of $\overline{H}H$ and PsPn gives a resonance state whose lifetime is estimated to be 16 fs. An adiabatic treatment gives a molecule with infinite lifetime against dissociation; therefore, a non-adiabatic calculation including dissociation channels is required to discuss the stability of $\overline{H}H$.

An effect of the rearrangement between $\overline{H}$ + H and Ps + Pn channels is investigated by the fragment channel wavefunctions. The channel wavefunction of the $\overline{H}$ + H configuration gives a narrow resonance width and relatively long lifetime. Mixing of the two configurations makes the $\overline{H}H$ molecular resonance states unstable. The attractive interaction of the $\overline{H}H$ is shorter than that of H_2 and hence the channel wavefunction of $\overline{H}$ + H configuration gives a more sparse density of resonance states in $\overline{H}H$ than the density of bound states in H_2. Besides, the rearrangement effect is unique for $\overline{H}H$ in comparison with H_2 and ordinary molecules consisting of particles.

Resonance states located near the threshold would affect the low energy scattering cross section [36, 37]. Thus, an accurate calculation of the molecular resonance state of $\overline{\mathrm{H}}\mathrm{H}$ can contribute to low energy antihydrogen experiments where the $\overline{\mathrm{H}}$ + H reaction occurs [36, 38–40]. A detailed calculation including inter-particle correlations with higher angular momenta is now in progress. The inter-particle correlation with higher angular momenta in $\overline{\mathrm{H}}$ + H configuration can provide a more precise description of the Van der Waals interaction between $\overline{\mathrm{H}}$ and H. On the other hand, such inter-particle correlation in the Ps + Pn configuration can introduce different dissociation channels and would shorten the lifetime of the resonance states. It could be possible that the energy spectrum of resonance states of $\overline{\mathrm{H}}\mathrm{H}$ near the $\overline{\mathrm{H}}$ (1s) + H (1s) dissociation threshold is different from that of bound states of H_2 near the H (1s) + H (1s) dissociation threshold because the same trial wavefunction used in this work gives a different tendency in the complex scaling trajectories near the dissociation threshold. In future work, the nuclear force and annihilation effect should be investigated because in the S-wave state, the probability that the antiproton and proton contacts in the resonance state could be significant. Previous scattering calculations for $\overline{\mathrm{H}}$ + H [36] and $\overline{\mathrm{p}}$ + H [41] indicate the importance of the nuclear force and annihilation effects.

Acknowledgment

This work was financially supported by JSPS KAKENHI Grant Number JP17K05592, Grant-in-Aid for JSPS Research Fellow Grant Number JP16J02658, and Grant-in-Aid from the Division for Interdisciplinary Advanced Research and Education (DIARE), Tohoku University. The computation was partially conducted on the supercomputers at Kyushu University.

References

[1] T. Walcher, Annu. Rev. Nucl. Part. Sci. **38** 67 (1988).
[2] C. Amsler and F. Myhrer, Annu. Rev. Nucl. Part. Sci. **41** 219 (1991).
[3] Y. C. Jean, P. E. Mallon and D. M. Schrader, *Principles and Applications of Positron and Positronium Chemistry* (World Scientific, Singapore, 2003).
[4] C. M. Surko and F. A. Gianturco, *New Directions in Antimatter Physics and Chemistry* (Kluwer Academic Publishers, Netherlands, 2001).
[5] G. G. Ryzhikh and J. Mitroy, Phys. Rev. Lett. **79** 4124 (1997).
[6] K. Strasburger and H. Chojnacki, J. Chem. Phys. **108** 3218 (1998).
[7] J. Mitroy, M. W. J. Bromley and G. G. Ryzhikh, J. Phys. B: At. Mol. Opt. Phys. **32** 2203 (1999).
[8] J. Mitroy, M. W. J. Bromley and G. G. Ryzhikh, J. Phys. B: At. Mol. Opt. Phys. **35** R81 (2002).
[9] M. W. J. Bromley and J. Mitroy, Phys. Rev. A **66** 062504 (2002).
[10] Y. Kubota and Y. Kino, New J. Phys. **10** 023038 (2008).
[11] T. Yamashita, M. Umair and Y. Kino, J. Phys. B: At. Mol. Opt. Phys. **50** 205002 (2017).
[12] D. B. Cassidy and A. P. Mills, Nature **449** 195 (2007).
[13] M. Amoretti, C. Amsler, G. Bonomi, A. Bouchta, P. Bowe, C. Carraro, C. L. Cesar, M. Charlton, M. J. T. Collier, M. Doser, V. Filippini, K. S. Fine, A. Fontana, M. C. Fujiwara, R. Funakoshi, P. Genova, J. S. Hangst, R. S. Hayano, M. H. Holzscheiter, L. V. Jorgensen, V. Lagomarsino, R. Landua, D. Lindelöf, E. Lodi Rizzini, M. Macrì, N. Madsen, G. Manuzio, M. Marchesotti, P. Montagna, H. Pruys, C. Regenfus, P. Riedler, J. Rochet, A. Rotondi, G. Rouleau, G. Testera, A. Variola, T. L. Watson and D. P. van der Werf, Nature **419** 456 (2002).
[14] The ALPHA Collaboration, Nat. Phys. **7** 558 (2011).
[15] N. Kuroda, S. Ulmer, D. J. Murtagh, S. Van Gorp, Y. Nagata, M. Diermaier, S. Federmann, M. Leali, C. Malbrunot, V. Mascagna, O. Massiczek, K. Michishio, T. Mizutani, A. Mohri, H. Nagahama, M. Ohtsuka, B. Radics, S. Sakurai, C. Sauerzopf, K. Suzuki, M. Tajima, H. A. Torii, L. Venturelli, B. Wünschek, J. Zmeskal, N. Zurlo, H. Higaki, Y. Kanai, E. Lodi Rizzini, Y. Nagashima, Y. Matsuda, E. Widmann and Y. Yamazaki, Nat. Commun. **5** 4089 (2014).
[16] M. Diermaier, C. B. Jepsen, B. Kolbinger, C. Malbrunot, O. Massiczek, C. Sauerzopf, M. C. Simon, J. Zmeskal and E. Widmann, Nat. Commun. **8** 15749 (2017).

[17] M. Ahmadi, B. X. R. Alves, C. J. Baker, W. Bertsche, E. Butler, A. Capra, C. Carruth, C. L. Cesar, M. Charlton, S. Cohen, R. Collister, S. Eriksson, A. Evans, N. Evetts, J. Fajans, T. Friesen, M. C. Fujiwara, D. R. Gill, A. Gutierrez, J. S. Hangst, W. N. Hardy, M. E. Hayden, C. A. Isaac, A. Ishida, M. A. Johnson, S. A. Jones, S. Jonsell, L. Kurchaninov, N. Madsen, M. Mathers, D. Maxwell, J. T. K. McKenna, S. Menary, J. M. Michan, T. Momose, J. J. Munich, P. Nolan, K. Olchanski, A. Olin, P. Pusa, C. Ø. Rasmussen, F. Robicheaux, R. L. Sacramento, M. Sameed, E. Sarid, D. M. Silveira, S. Stracka, G. Stutter, C. So, T. D. Tharp, J. E. Thompson, R. I. Thompson, D. P. van der Werf and J. S. Wurtele, Nature **541** 506 (2016).
[18] M. Ahmadi, B. X. R. Alves, C. J. Baker, W. Bertsche, E. Butler, A. Capra, C. Carruth, C. L. Cesar, M. Charlton, S. Cohen, R. Collister, S. Eriksson, A. Evans, N. Evetts, J. Fajans, T. Friesen, M. C. Fujiwara, D. R. Gill, A. Gutierrez, J. S. Hangst, W. N. Hardy, M. E. Hayden, C. A. Isaac, A. Ishida, M. A. Johnson, S. A. Jones, S. Jonsell, L. Kurchaninov, N. Madsen, M. Mathers, D. Maxwell, J. T. K. McKenna, S. Menary, J. M. Michan, T. Momose, J. J. Munich, P. Nolan, K. Olchanski, A. Olin, P. Pusa, C. Ø. Rasmussen, F. Robicheaux, R. L. Sacramento, M. Sameed, E. Sarid, D. M. Silveira, S. Stracka, G. Stutter, C. So, T. D. Tharp, J. E. Thompson, R. I. Thompson, D. P. van der Werf and J. S. Wurtele, Nature **548** 66 (2017).
[19] M. Ahmadi, B. X. R. Alves, C. J. Baker, W. Bertsche, A. Capra, C. Carruth, C. L. Cesar, M. Charlton, S. Cohen, R. Collister, S. Eriksson, A. Evans, N. Evetts, J. Fajans, T. Friesen, M. C. Fujiwara, D. R. Gill, J. S. Hangst, W. N. Hardy, M. E. Hayden, C. A. Isaac, M. A. Johnson, J. M. Jones, S. A. Jones, S. Jonsell, A. Khramov, P. Knapp, L. Kurchaninov, N. Madsen, D. Maxwell, J. T. K. McKenna, S. Menary, T. Momose, J. J. Munich, K. Olchanski, A. Olin, P. Pusa, C. Ø. Rasmussen, F. Robicheaux, R. L. Sacramento, M. Sameed, E. Sarid, D. M. Silveira, G. Stutter, C. So, T. D. Tharp, R. I. Thompson, D. P. van der Werf and J. S. Wurtele, Nature **557** 71 (2018).
[20] Y. Sacquin, Eur. Phys. J. D **68** 31 (2014).
[21] P. Scampoli and J. Storey, Mod. Phys. Lett. A **29** 1430017 (2014).
[22] Y. K. Ho, Phys. Rev. A **17** 1675 (1978).
[23] A. M. Frolov and V. H. Smith, Jr., Phys. Rev. A **56** 2417 (1997).
[24] S. L. Saito, Nucl. Instr. Meth. Phys. Res. B **171** 60 (2000).
[25] S. Bubin and L. Adamowicz, Phys. Rev. A **74** 052502 (2006).
[26] S. Bubin and K. Varga, Phys. Rev. A **84** 012509 (2011).
[27] T. Yamashita, Y. Kino, E. Hiyama, S. Jonsell and P. Froelich, J. Phys.: Conf. Ser. **875** 052031 (2017).
[28] H. Stegeby, K. Piszczatowski, H. Karlsson, R. Lindh and P. Froelich, Cent. Eur. J. Phys. **10** 1038 (2012).
[29] H. Stegeby and K. Piszczatowski, J. Phys. B: At. Mol. Opt. Phys. **49** 014002 (2016).
[30] E. Hiyama, Y. Kino and M. Kamimura, Prog. Part. Nucl. Phys. **51** 223 (2003).
[31] T. Yamashita and Y. Kino, Eur. Phys. J. D **72** 13 (2018).
[32] T. Yamashita and Y. Kino, Eur. Phys. J. Web Conf. **181** 01034 (2018).
[33] Y. K. Ho, Phys. Rep. **99** 1 (1983).
[34] K. Piszczatowski, G. Łach, M. Przybytek, J. Komasa, K. Pachucki and B. Jeziorski, J. Chem. Theory Comput. **5** 3039 (2009).
[35] K. Strasburger, J. Phys. B: At. Mol. Opt. Phys. **35** L435 (2002).
[36] A. Y. Voronin and P. Froelich, Phys. Rev. A **77** 022505 (2008).
[37] E. Garrido, D. V. Fedorov and A. S. Jensen, Phys. Lett. B **684** 132 (2010).
[38] A. Voronin and J. Carbonell, Hyperfine Interact. **115** 143 (1998).
[39] P. Froelich, S. Jonsell, A. Saenz, B. Zygelman and A. Dalgarno, Phys. Rev. Lett. **84** 4577 (2000).
[40] B. Zygelman, A. Saenz, P. Froelich and S. Jonsell, Phys. Rev. A **69** 042715 (2004).
[41] K. Sakimoto, Phys. Rev. A **90** 032514 (2014).